Inorganic Chemistry
Article

Inorg. Chem. **2010**, *49*, 10013–10021 **10013**
DOI: 10.1021/ic101316u

Crystal Chemistry of the Noncentrosymmetric Eulytites: $A_3Bi(XO_4)_3$ (X = V, A = Pb; X = P, A = Ca, Cd, Sr, Pb)

Prangya Parimita Sahoo and T. N. Guru Row*

Solid State and Structural Chemistry Unit, Indian Institute of Science, Bangalore 560012, India

Received July 3, 2010

Eulytite compounds, $A_3Bi(XO_4)_3$ (X = P, A = Ca, Cd, Sr, Pb), belong to the noncentrosymmetric space group $I\bar{4}3d$ (No. 220) as determined by single-crystal X-ray diffraction studies. The crystals were grown from the melt−cool technique with considerable difficulty as the compounds melt incongruently at their melting temperature, except for the compound $Pb_3Bi(PO_4)_3$. The unit cell parameter *a* is 9.984(5), 9.8611(3), 10.2035(3), and 10.3722(2) Å for $Ca_3Bi(PO_4)_3$, $Cd_3Bi(PO_4)_3$, $Sr_3Bi(PO_4)_3$, and $Pb_3Bi(PO_4)_3$ respectively, and there are four formula units in the unit cell. The structure of $Pb_3Bi(VO_4)_3$, a unique eulytite with vanadium substitution, is compared with all these phosphorus substituted eulytites. The A^{2+} and Bi^{3+} cations occupy the special position (16*c*) while the O anions occupy the general Wyckoff position (48*e*) in the crystal structure. Only one O position has been identified for $Pb_3Bi(PO_4)_3$ and $Pb_3Bi(VO_4)_3$, whereas two O atom sites were identified for $Ca_3Bi(PO_4)_3$, $Cd_3Bi(PO_4)_3$, and $Sr_3Bi(PO_4)_3$. The UV−vis diffuse reflectance spectra indicate large band gaps for all the phosphate eulytites while a lower band gap is observed for the vanadate eulytite. The feasibility of the use of these compounds in optoelectronic devices has been tested by measuring the second-harmonic generation (SHG) values which have been found to be of a magnitude equivalent to the commercially used KDP (KH_2PO_4).

Introduction

Compounds crystallizing in the 21 noncentrosymmetric (NCS) crystal classes have been of considerable interest because of their propensity to display a wide range of symmetry based properties like ferroelectricity, pyroelectricity, piezoelectricity, and second order nonlinear optical (NLO) behavior. Compounds displaying NLO activity find applications as second-harmonic generators and electro-optical and photorefractive devices and in optical communication and signal processing.[1−3] In recent years, attempts to synthesize compounds, which crystallize in noncentrosymmetric space groups to ensure NLO behavior, have been made, specially with borates and phosphates. The most commonly used NLO materials are borates like β-BaB_2O_4 (BBO) and LiB_3O_5 (LBO) and phosphates like KH_2PO_4 (KDP) and $KTiOPO_4$ (KTP).[4−7]

The mineral $Bi_4(SiO_4)_3$ (BSO) was discovered in association with elemental bismuth and quartz and is the first member of the eulytite class of compounds crystallizing in the noncentrosymmetric space group $I\bar{4}3d$ with four formula units in the unit cell.[8] Single crystals of BSO and its germanate analogue $Bi_4(GeO_4)_3$ (BGO) have been grown by Czochralski and vertical Bridgman methods[9−11] and have been studied in detail, owing to their property to act as a scintillation detector.[12−16] Electro-optic, electro-mechanic, and luminescence properties of BGO and BSO have also been discussed in the literature,[17−20] and recently, theoretical calculations have shown the propensity of these materials to act as radiation energy absorbers.[21] A series of compounds have been synthesized with proper substitutions at Bi and Si/Ge sites in these systems. They are $A_3B(XO_4)_3$, $A_7C(XO_4)_6$, and $A'_3A_5(XO_4)_6$ where A = divalent cation, A′ = monovalent cation, B = trivalent cation, C = tetravalent cation, and X = pentavalent

*To whom correspondence should be addressed. E-mail: ssctng@sscu.iisc.ernet.in. Phone: +91-80-22932796. Fax: +91-80-23601310.

(1) Becker, P. *Adv. Mater.* **1998**, *10*, 979.
(2) Halasyamani, P. S.; Poeppelmeier, K. R. *Chem. Mater.* **1998**, *10*, 2753.
(3) Ok, K. M.; Chi, E. O.; Halasyamani, P. S. *Chem. Soc. Rev.* **2006**, *35*, 710.
(4) Chen, C. T.; Wu, B. C.; Jiang, A. D.; You, G. M. *Sci. Sin. B* **1985**, *28*, 235.
(5) Chen, C. T.; Wu, Y. C.; Jiang, A. D.; Wu, B. C.; You, G. M.; Li, R. K.; Lin, S. J. *J. Opt. Soc. Am. B* **1989**, *6*, 616.
(6) Hagen, W. F.; Magnante, P. C. *J. Appl. Phys.* **1969**, *40*, 219.
(7) Zumsteg, F. C.; Bierlein, J. D.; Gier, T. E. *J. Appl. Phys.* **1976**, *47*, 4980.
(8) Menzer, G. *Z. Kristallogr.* **1931**, *78*, 136.
(9) Liebertz, J. *J. Cryst. Growth* **1969**, *5*, 150.
(10) Philipsborn, H. v. *J. Cryst. Growth* **1971**, *11*, 348.
(11) van Enckevort, W. J. P.; Smet, F. *J. Cryst. Growth* **1990**, *102*, 314.
(12) Weber, M. J.; Monchamp, R. R. *J. Appl. Phys.* **1973**, *44*, 5495.
(13) Nestor, O. H.; Huang, C. Y. *IEEE Trans. Nucl. Sci.* **1975**, *Ns22*, 68.
(14) Feng, X. Q.; Hu, G. Q.; Yin, Z. W.; Huang, Y. P.; Kapphan, S.; Fisher, C.; Zhou, F. Z.; Yang, Y.; Fan, D. Y. *Mater. Sci. Eng., B* **1994**, *23*, 83.
(15) Ishii, M.; Harada, K.; Hirose, Y.; Senguttuvan, N.; Kobayashi, M.; Yamaga, I.; Ueno, H.; Miwa, K.; Shiji, F.; Yiting, F.; Nikl, M.; Feng, X. Q. *Opt. Mater.* **2002**, *19*, 201.
(16) Blasse, G. *Chem. Mater.* **1994**, *6*, 1465.
(17) Bortfeld, D. P.; Meier, H. *J. Appl. Phys.* **1972**, *43*, 5110.
(18) Schweppe, H. *IEEE Trans. Son. Ultrason.* **1969**, *Su16*, 219.
(19) Moncorge, R.; Jacquier, B.; Boulon, G. *J. Lumin.* **1976**, *14*, 337.
(20) Moncorge, R.; Jacquier, B.; Boulon, G.; Gaumemahn, F.; Janin, J. *J. Lumin.* **1976**, *12*, 467.
(21) Lalic, M. V.; Souza, S. O. *Opt. Mater.* **2008**, *30*, 1189.

Published on Web 09/27/2010

cation.[22−29] $Pb_4(PO_4)_2CrO_4$ and $Pb_4(PO_4)_2SO_4$ are some examples of eulytites with mixed tetrahedral site cations.[30,31] Eulytites containing rare earths have also been studied in detail for their luminescent properties.[25,32−35] Second-harmonic generation (SHG) measurements on $Pb_3Bi(PO_4)_3$, $Ba_3Bi(PO_4)_3$, and $La_3Bi(PO_4)_3$ show significant activity.[36] Cations like Tl^+, Pb^{2+}, and Bi^{3+} possess stereochemically active "$6s^2$" lone pairs of electrons resulting in a distorted co-ordination environment.[37] However, in spite of advances in the research related to eulytites, the number of single-crystal structure determinations has been sparse. The main reason for scantly available single-crystal data on eulytites is the inherent difficulty associated with growing the single crystals due to their incongruent melting point, thermal instabilities, etc. To the best of our knowledge, the eulytites whose single-crystal structures have been determined are BGO, BSO, $Pb_4(PO_4)_2(SO_4)$, $Ba_3Bi(PO_4)_3$, $Na_3Bi_5(PO_4)_6$, $Pb_3V(PO_4)_3$, $Pb_3Bi(VO_4)_3$, and $Pb_3Bi(PO_4)_3$.[27,30,36,38−40] In our recent article, the difficulty associated with the crystal growth of the eulytite $Pb_3Bi(VO_4)_3$ has been discussed.[40]

The local structural features reveal the presence of both cationic and anionic disorder in most of the eulytites which are reflected in the resulting associated properties. It is, hence, required to determine structures of a reasonable number of eulytites to understand the underlying structure−property correlation. In fact, eulytites have been classified into four categories based on the disorder features associated with both cationic and anionic sites in a systematic study of known eulytite structures.[39] In order to gain a better insight into the details of structural features and to evaluate the extent of disorder at atomic sites, it is required that studies be restricted to good quality single crystals. In this context, we present the synthesis and characterization of the eulytites $A_3Bi(XO_4)_3$ (X = V, A = Pb; X = P, A = Ca, Cd, Sr, Pb) in the phase diagram of $A_3(XO_4)_2$-$BiXO_4$. In all cases, quality single crystals were grown which facilitates the identification of subtle differences in the coordination environment in various eulytites. We also report the details of the relevant laboratory powder X-ray diffraction (XRD), variable temperature synchrotron powder XRD, solid-state UV−vis diffuse reflectance spectra and SHG activity of the eulytites described in this Article.

Experimental Section

Materials. Bi_2O_3 (Aldrich, 99.9%) was dried at 350 °C for 6 h before use. PbO (Aldrich, 99.9%), $SrCO_3$, $CaCO_3$, $Cd(CH_3COO)_2 \cdot 2H_2O$, and $(NH_4)_2HPO_4$ (all from S. D. Fine-Chem Ltd., India, 99%) were used as received.

Preparation and Crystal Growth. Polycrystalline samples of phases $A_3Bi(PO_4)_3$ (A = Ca, Cd, Sr, Pb) were synthesized by the solid-state route using stoichiometric amounts of the starting materials $CaCO_3$, $Cd(CH_3COO)_2 \cdot 2H_2O$, $SrCO_3$, PbO, and $(NH_4)_2HPO_4$. The compositions of the starting reactants were initially ground well in an agate mortar and pestle. The resultant mixture was fired at 300 °C for 6 h to expel NH_3. Then, it was ground well and again put for heat treatment at 650 °C for 8 h to decompose the carbonate and the acetate. The eulytite phases were synthesized at 855 °C for 12 h and 950 °C for 12 h for $Ca_3Bi(PO_4)_3$, 800 °C for 10 h and 980 °C for 12 h for $Cd_3Bi(PO_4)_3$, 1100 °C for 12 h for $Sr_3Bi(PO_4)_3$, and 875 °C for 6 h for $Pb_3Bi(PO_4)_3$. All the syntheses were carried out under oxygen atmosphere. The color of the products obtained was white. The progress of the reaction was monitored by powder XRD. Pure phases were synthesized for $Ca_3Bi(PO_4)_3$, $Sr_3Bi(PO_4)_3$, and $Pb_3Bi(PO_4)_3$, but a pure phase could not be obtained for $Cd_3Bi(PO_4)_3$. $Pb_3Bi(VO_4)_3$ was synthesized as per the method given in the literature.[40]

Single crystals of the compounds $A_3Bi(PO_4)_3$ (A = Ca, Cd, Sr, Pb) were obtained by the melt−cool technique at various temperature ranges (Scheme 1). The features of the incongruent melting character of these compounds manifest as deterrents to produce quality crystals. However, a programmed approach as shown in Scheme 1 and later described in the Results and Discussion section allows for the isolation of good quality single crystals suitable for X-ray diffraction studies.

Powder XRD. Powder XRD data were collected using a Philips X-pert diffractometer with Cu Kα radiation over the angular range $5° \le 2\theta \le 110°$, with a step width of 0.0167° at room temperature calibrated against Silicon Powder (NIST-SRM 640c) standards. Le Bail profile analysis in the *JANA2000* suite of programs was used to refine the XRD data.[41] The background was estimated by a Legendre polynomial function consisting of 15 coefficients, and the peak shapes were described by a pseudo-Voigt function varying five profile coefficients. A scale factor, a zero error factor, and shape were also refined.

Variable-temperature powder XRD data were collected at the synchrotron source at Trieste, Italy. The wavelength used for the experiment was 1.0 Å, calibrated against LaB_6 (NIST-SRM 660a) standards. The samples were loaded in a capillary after sonication. The capillary was rotated during data accumulation. The program *Fit2d* was used to integrate the data obtained from the synchrotron source.[42]

Single-Crystal XRD. Colorless single crystals (Figure S1 in the Supporting Information) were selected on the basis of size and sharpness of diffraction spots. Data collection was carried out on an Oxford Xcalibur MOVA diffractometer with a four-circle κ goniometer and equipped with an EOS CCD detector using graphite-monochromatized Mo Kα ($\lambda_{Mo\ K\alpha} = 0.71073$ Å) radiation at 293 (2) K, except for $Cd_3Bi(PO_4)_3$, for which data were collected at 115(1) K. The diffraction intensities were corrected for Lorentz and polarization effects. The data were reduced using CrysAlis RED (special programs available with the diffractometer); the shape was determined with the video microscope attached to the diffractometer, and an analytical absorption correction (after Clark and Reid) was applied. The structures were solved by direct

(22) Blasse, G. *J. Solid State Chem.* **1970**, *2*, 27.
(23) Perret, R.; Damak, M. *J. Less-Common Met.* **1985**, *108*, 23.
(24) Fukuda, K.; Matsubara, H.; Fukutani, K.; Yoshida, H. *Powder Diffr.* **2004**, *19*, 385.
(25) Liang, H. B.; Tao, Y.; Su, Q. *Mater. Sci. Eng., B* **2005**, *119*, 152.
(26) Fukuda, K.; Wata, T.; Niwa, T. *J. Solid State Chem.* **2006**, *179*, 3420.
(27) Shpanchenko, R. V.; Panin, R. V.; Hadermann, J.; Bougerol, C.; Takayama-Muromachi, E.; Antipov, E. V. *J. Solid State Chem.* **2005**, *178*, 3715.
(28) Engel, G. *Z. Anorg. Allg. Chem.* **1972**, *387*, 22.
(29) Szuszkiewicz, W.; Znamierowska, T. *J. Solid State Chem.* **1990**, *88*, 406.
(30) Barbier, J. *Eur. J. Solid State Inorg. Chem.* **1994**, *31*, 163.
(31) Barbier, J.; Maxin, D. *J. Solid State Chem.* **1995**, *116*, 179.
(32) Folkerts, H. F.; Zuidema, J.; Blasse, G. *Chem. Phys. Lett.* **1996**, *249*, 59.
(33) Liang, H. B.; Tao, Y.; Xu, J. H.; He, H.; Wu, H.; Chen, W. X.; Wang, S. B.; Su, Q. *J. Solid State Chem.* **2004**, *177*, 901.
(34) Hoogendorp, M. F.; Schipper, W. J.; Blasse, G. *J. Alloys Compd.* **1994**, *205*, 249.
(35) Xiao, X. Z.; Xu, S.; Yan, B. *J. Alloys Compd.* **2007**, *429*, 255.
(36) Zhang, W. L.; Lin, X. S.; Zhang, H.; Wang, J. Y.; Lin, C. S.; He, Z. Z.; Cheng, W. D. *Dalton Trans.* **2010**, *39*, 1546.
(37) Orgel, L. E. *J. Chem. Soc.* **1959**, 3815.
(38) Arbib, E.; Chaminade, J. P.; Darriet, J.; Elouadi, B. *Solid State Sci.* **2000**, *2*, 243.
(39) Arbib, E.; Elouadi, B.; Chaminade, J. P.; Darriet, J. *Mater. Res. Bull.* **2000**, *35*, 761.
(40) Sahoo, P. P.; Gaudin, E.; Darriet, J.; Row, T. N. G. *Mater. Res. Bull.* **2009**, *44*, 812.
(41) Dusek, M.; Petricek, V.; Wunschel, M.; Dinnebier, R. E.; van Smaalen, S. *J. Appl. Crystallogr.* **2001**, *34*, 398.
(42) Hammersley, A. P. FIT2D V6.4 Reference Manual V1.18, ESRF Internal Report, EXP/AH/95-01, **1995**.

Scheme 1

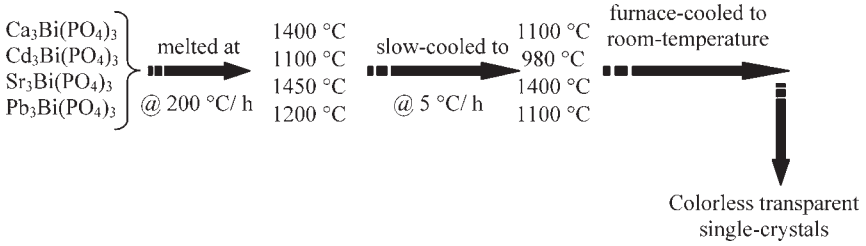

Table 1. Principal Characteristics of $A_3Bi(PO_4)_3$ (A = Pb, Ca, Sr, Cd) Single-Crystal XRD Structure Determination

chemical formula	$Ca_3Bi(PO_4)_3$	$Cd_3Bi(PO_4)_3$	$Sr_3Bi(PO_4)_3$	$Pb_3Bi(PO_4)_3$
formula weight	614.3	831.09	756.75	1115.46
crystal habit, color	plate, white	irregular, white	block, white	plate, white
crystal size/mm	0.005 × 0.002 × 0.001	0.03 × 0.02 × 0.01	0.011 × 0.003 × 0.001	0.112 × 0.088 × 0.043
temperature/K	293(2)	115(1)	293(2)	293(2)
wavelength/Å	0.71073 (Mo Kα)	0.71073 (Mo Kα)	0.71073 (Mo Kα)	0.71073 (Mo Kα)
monochromator	graphite	graphite	graphite	graphite
crystal system	cubic	cubic	cubic	cubic
space group	$I\bar{4}3d$	$I\bar{4}3d$	$I\bar{4}3d$	$I\bar{4}3d$
a/Å	9.984(5)	9.8611(3)	10.2035(3)	10.3722(2)
volume/Å^3	995.2(9)	958.92(5)	1062.31(6)	1115.87(4)
Z	4	4	4	4
density/g cm^{-3}	4.099	5.757	4.732	6.672
$F(000)$	1136	1472	1352	1880
scan mode	ω scan	ω scan	ω scan	ω scan
θmax (°)	32.35	29.26	32.4120	32.5784
$h_{min,max}$, $k_{min,max}$, $l_{min,max}$	(−15, 10), (−14, 13), (−5, 15)	(−8, 13),(−7, 12), (−12, 12)	(−15, 14), (−15, 13), (−15, 14)	(−15, 15), (−15, 15), (−15, 15)
no. of reflns measured	1386	980	2972	705
no. of unique reflns	257	186	318	266
absorption correction	analytical from crystal shape	analytical from crystal shape	analytical from crystal shape	analytical from crystal shape
μ (mm^{-1})	19.811	25.429	32.013	61.341
no. of parameters	26	15	26	16
refinement	F^2	F^2	F^2	F^2
R_all, R_obs	0.0235, 0.0180	0.0308, 0.0287	0.0327, 0.0282	0.0313 0.0274
wR_2_all, wR_2_obs	0.0320, 0.0315	0.0684, 0.0678	0.0645,0.0638	0.0644,0.0636
GoF	1.096	1.095	1.063	1.042
max, min $\Delta\rho$ e/Å^3	0.362, −0.497	0.751, −0.529	0.738, −0.636	1.744, −1.837

methods using *SHELXS97* and refined using *SHELXL97* included in the package WinGX, from 231, 186, 241, and 285 independent reflections, having $I \geq 2\sigma(I)$ for $Ca_3BiP_3O_{12}$, $Cd_3BiP_3O_{12}$, $Pb_3BiP_3O_{12}$, and $Sr_3BiP_3O_{12}$, respectively.[43,44] The crystal data have been deposited at the Fachinformationszentrum Karlsruhe (FIZ) with the numbers CSD 420843, 380462, 380463, and 380464 for $Pb_3Bi(PO_4)_3$, $Sr_3Bi(PO_4)_3$, $Ca_3Bi(PO_4)_3$, and $Cd_3Bi(PO_4)_3$, respectively. The packing diagrams were generated by *DIAMOND* version 2.1c.[45] Crystallographic data and the details of the single-crystal data collection are given in Table 1. Atomic coordinates and isotropic displacement parameters are presented in Table 2. Anisotropic displacement parameters (ADPs) and selected interatomic distances and angles are given in Tables 3 and 4.

UV−Vis and Second Harmonic Generation Measurements. UV−vis diffuse-reflectance spectra were recorded at room temperature, on a Perkin-Elmer Lambda 35 UV−vis Spectrophotometer, from 200 to 800 nm. The $BaSO_4$ plate was used as a standard.

Frequency doubling experiments were carried out on powdered samples of $A_3Bi(XO_4)_3$ (X = P, A = Ca, Cd, Sr, P) and $Pb_3Bi(VO_4)_3$ based on the Kurtz and Perry method.[46,47] Q-switched Nd:YAG laser of fundamental wavelength 1064 nm (Spectra Physics, PRO-LAB 170, pulse width of 10 ns and repetition rate of 10 Hz) was used as the source of light for SHG experiment. The beam from the laser was passed through a couple of high energy laser mirrors (Melles Griot, 99.9% reflection) and a glass filter (RG 645, to reject the light from the flash lamp of laser) before being focused. The energy of the laser beam was kept at 2.4 mJ/pulse. The incident beam power was measured using a power meter (Scientech Vector H410). The beam was focused into a glass capillary, using a converging lens of 200 mm focal length. The incoherently scattered SH photons were collected in the transverse direction using a combination of a monochromator (Triax 550, Jobin Yvon, 0.024 nm resolution, 5 mm entrance and exit slit widths) and a photomultiplier tube (Hamamatsu, R2059). The second harmonic signal was then sampled, averaged over 512 shots, and recorded in a digital storage oscilloscope (Tektronix TDS 3520B).

Results and Discussion

Crystal Structures. $Ca_3Bi(PO_4)_3$, $Cd_3Bi(PO_4)_3$, $Sr_3Bi(PO_4)_3$, and $Pb_3Bi(PO_4)_3$ were indexed in a cubic crystal system with $a = 9.984(5)$ Å, $V = 995.2(9)$ Å^3; $a = 9.8611(3)$ Å, $V = 958.92(5)$ Å^3; $a = 10.2035(3)$ Å, $V = 1062.31(6)$ Å^3; and $a = 10.3722(2)$ Å, $V = 1115.87(4)$ Å^3, respectively. Space group $I\bar{4}3d$ (No. 220) was assigned on the basis of systematic absences. A gradual increase observed for the cell parameter is commensurate with the increase in ionic radii of the A cation (Figure 1).

The positions of the heavy atoms were obtained by direct methods. The location of the O atoms was based on the difference Fourier synthesis after locating and refining all

(43) Sheldrick, G. M. *Acta Cryst. A* **2008**, *64*, 112.
(44) Farrugia, L. J. *J. Appl. Crystallogr.* **1999**, *32*, 837.
(45) Brandenburg, K. *DIAMOND, Version. 2.1c*; Crystal Impact GbR: Bonn, Germany, 1999.
(46) Kurtz, S. K.; Perry, T. T. *J. Appl. Phys.* **1968**, *39*, 3798.
(47) Dougherty, J. P.; Kurtz, S. K. *J. Appl. Crystallogr.* **1976**, *9*, 145.

Table 2. Atomic Coordinates (Å) and Isotropic Displacement Parameters (Å^2) for $A_3Bi(PO_4)_3$ (A = Pb, Ca, Sr, Cd) Obtained from Single-Crystal XRD

atomic and Wyckoff position	*x*	*y*	*z*	*Ueq* (Å^2)	occupancy
		$Ca_3Bi(PO_4)_3$			
Ca/Bi (16*c*)	0.07319(3)	*x*	*x*	0.01848(15)	0.75/0.25
P (12*b*)	0	0.75	0.125	0.0169(3)	1
O1[a] (48*e*)	0.1244(7)	0.7189(15)	0.0405(4)	0.040(3)	0.75(3)
O2[a] (48*e*)	0.085(3)	0.656(2)	0.0425(16)	0.045(5)	0.25(3)
		$Cd_3Bi(PO_4)_3$			
Cd/Bi (16*c*)	0.17525(5)	*x*	*x*	0.0297(3)	0.75/0.25
P (12*b*)	0.5	0.25	0.125	0.0308(10)	1
O1[b] (48*e*)	0.5274(19)	0.1221(16)	0.2055(13)	0.065(5)	0.81(5)
O2[b] (48*e*)	0.600(9)	0.166(8)	0.206(5)	0.07(3)	0.19(5)
		$Sr_3Bi(PO_4)_3$			
Sr/Bi (16*c*)	0.18047(4)	*x*	*x*	0.0253(2)	0.75/0.25
P (12*b*)	0.25	0.125	0.5	0.0181(5)	1
O1[a] (48*e*)	0.317(4)	0.0429(10)	0.605(2)	0.055(8)	0.65(8)
O2[a] (48*e*)	0.239(7)	0.0401(18)	0.622(2)	0.052(12)	0.35(8)
		$Pb_3Bi(PO_4)_3$			
Pb/Bi (16*c*)	0.17462(3)	*x*	*x*	0.0151 (2)	0.75/0.25
P (12*b*)	0.25	−0.125	0	0.0119(9)	1
O (48*e*)	0.1984(10)	−0.0407(8)	0.1107(9)	0.026(2)	1

[a] All split atoms have been treated using the PART command in the refinement to ensure that the thermal parameters and occupancy factors are not refined together. [b] These two split atoms are refined isotropically.

Table 3. Atomic Coordinates (Å) and Isotropic Displacement Parameters (Å^2) for $A_3Bi(PO_4)_3$ (A = Pb, Ca, Sr, Cd) Obtained from Single-Crystal XRD

atomic and Wyckoff position	U_{11}	U_{22}	U_{33}	U_{23}	U_{13}	U_{12}
			$Ca_3Bi(PO_4)_3$			
Ca/Bi (16*c*)	0.01848(15)	U_{11}	U_{11}	−0.00036(12)	U_{23}	U_{23}
P (12*b*)	0.0181(5)	U_{11}	0.0147(7)	0	0	0
O1 (48*e*)	0.023(2)	0.075(7)	0.022(2)	0.001(2)	0.0020(17)	0.017(3)
O2 (48*e*)	0.040(9)	0.016(8)	0.079(11)	0.001(6)	0.037(8)	0.010(7)
			$Cd_3Bi(PO_4)_3$			
Cd/Bi (16*c*)	0.0297(3)	U_{11}	U_{11}	0.0016(3)	U_{23}	U_{23}
P (12*b*)	0.0368(13)	U_{11}	0.0179(18)	0	0	0
O1 (48*e*)						
O2 (48*e*)						
			$Sr_3Bi(PO_4)_3$			
Sr/Bi (16*c*)	0.0253(2)	U_{11}	U_{11}	0.00536(15)	U_{23}	U_{23}
P (12*b*)	0.0192(7)	0.0157(10)	U_{11}	0	0	0
O1 (48*e*)	0.082(17)	0.034(5)	0.048(8)	0.006(4)	−0.045(10)	0.002(6)
O2 (48*e*)	0.08(3)	0.035(9)	0.041(8)	0.011(7)	−0.003(11)	−0.006(11)
			$Pb_3Bi(PO_4)_3$			
Pb/Bi (16*c*)	0.0151(3)	U_{11}	U_{11}	0.0013(2)	U_{23}	U_{23}
P (12*b*)	0.0121(19)	0.0115(13)	U_{11}	0	0	0
O (48*e*)	0.040(3)	0.015(5)	0.024(4)	−0.003(4)	0.015(3)	0.008(3)

the heavy atoms and their displacement parameters. For the series $A_3Bi(XO_4)_3$ (X = P, A = Ca, Cd, Sr, Pb), the A/Bi atoms were located at the 16*c* Wyckoff site (3-fold axis). The final refinement of the structure was achieved using a fixed site occupancy ratio 3:1 for A and Bi, equal to the ideal values, in accordance with the chemical formula $A_3Bi(XO_4)_3$ (X = P, A = Ca, Cd, Sr, Pb). The atomic coordinates and thermal parameters of Bi were fixed to be the same as that of Ca/Cd/Sr/Pb in each case. The P atom was located at the 12*b* site (4 axis). For a phosphorus atom in P^{5+} state, the P−O distance is expected to be 1.55 Å from literature data. It is noteworthy that, considering this distance criterion, only one O atom site was located for the eulytite $Pb_3Bi(PO_4)_3$, whereas two O atom sites were located for the compounds $Ca_3Bi(PO_4)_3$, $Cd_3Bi(PO_4)_3$, and $Sr_3Bi(PO_4)_3$. The O atom(s) was/were located at the 48*e* Wyckoff site (general position). Because of the high displacement parameters of the oxygen atoms and high residual electron density, low temperature data (115 K) were collected on the $Cd_3Bi(PO_4)_3$ single crystal. The occupancies of the O atoms were allowed to be refined for $Ca_3Bi(PO_4)_3$, $Cd_3Bi(PO_4)_3$, and $Sr_3Bi(PO_4)_3$. Anisotropic refinements could be carried out for the oxygen atoms of all the eulytites except $Cd_3Bi(PO_4)_3$.The occupancies for the two partially occupied O atoms for $Ca_3Bi(PO_4)_3$, $Cd_3Bi(PO_4)_3$, and $Sr_3Bi(PO_4)_3$ were found to be in the ratios of 0.75(3):0.25(3),

Table 4. Selected Bond Lengths and Bond Angles for $A_3Bi(PO_4)_3$ (A = Pb, Ca, Sr, Cd) Obtained from Single-Crystal XRD

	bond length type	distances (Å)	bond angle type	angles (deg)
$Ca_3Bi(PO_4)_3$	P−O1	1.508(13) × 4	O1−P−O1	113.2(3) × 2
	−O2	1.533(5) × 4		107.62(15) × 4
			O2−P−O2	113.8(12) × 2
				107.4(6) × 4
	Ca/Bi−O1	2.271(4) × 3	O1−Ca/Bi−O1	67.8(3) × 3
		2.443(5) × 3		83.44(15) × 3
	Ca/Bi−O2	2.382(17) × 3		90.0(6) × 3
		2.74(3) × 3		114.12(12) × 3
				156.8(4) × 3
			O2−Ca/Bi−O2	62.3(12) × 3
				79.48(19) × 3
				83.0(8) × 3
				116.98(17) × 3
				136.7(9) × 3
$Cd_3Bi(PO_4)_3$	P−O1	1.514(14) × 4	O1−P−O1	116.8(10) × 2
	−O2	1.51(7) × 4		105.9(5) × 4
			O2−P−O2	116(4) × 2
				106.3(19) × 4
	Cd/Bi−O1	2.266(13) × 3	O1−Cd/Bi−O1	67.0(7) × 3
		2.377(14) × 3		84.7(3) × 3
	Cd/Bi−O2	2.72(7) × 3		92.4(7) × 3
		2.35(6) × 3		112.9(3) × 3
				159.0(5) × 3
			O2−Cd/Bi−O2	61(4) × 3
				80(2) × 3
				83(6) × 3
				117(2) × 3
				136(8) × 3
$Sr_3Bi(PO_4)_3$	P−O1	1.524(8) × 4	O1−P−O1	113.3(8) × 2
	-O2	1.520(19) × 4		107.6(4) × 4
			O2−P−O2	110.5 (16) × 2
				108.9(8) × 4
	Sr/Bi−O1	2.599(18) × 3	O1−Sr/Bi−O1	73.1(16) × 3
		2.405(14) × 3		75.9(8) × 3
	Sr/Bi−O1	2.47(3) × 3		80.1(2) × 3
		2.405(14) × 3		116.86(17) × 3
				143.7(12) × 3
			O2−Sr/Bi−O2	65.2(8) × 3
				84.1(5) × 3
				99.5(17) × 3
				164.7(14) × 3
				110.7(10) × 3
$Pb_3Bi(PO_4)_3$	P−O	1.539(9) × 4	O−P−O	108.8(5) × 4
				110.8 (5) × 2
	Pb/Bi−O	2.636(9) × 3	O−Pb/Bi−O	74.2(3) × 3
		2.343(8) × 3		82.0(3) × 3
				81.4(3) × 3
				114.5(3) × 3
				152.5(3) × 3

0.65(8):0.35(8), and 0.81(5):0.19(5), respectively. It is to be noted that NPD studies of $Ca_3Bi(PO_4)_3$ gave an occupancy ratio of 0.625(13):0.375(13). The final residual factors are $R_{\_obs} = 0.0180$ and $wR_{2\_obs} = 0.0315$ for $Ca_3Bi(PO_4)_3$, $R_{\_obs} = 0.0287$ and $wR_{2\_obs} = 0.0678$ for $Cd_3Bi(PO_4)_3$, $R_{\_obs} = 0.0282$ and $wR_{2\_obs} = 0.0638$ for $Sr_3Bi(PO_4)_3$, and $R_{\_obs} = 0.0274$ and $wR_{2\_obs} = 0.0636$ for $Pb_3Bi(PO_4)_3$. The crystal structure of $Pb_3Bi(VO_4)_3$ has already been published elsewhere, and the oxygen atom was confined to a single site.[40]

In general, eulytite structures consist of a three-dimensional packing of $[PO_4]^{3-}$ tetrahedra and $[BiO_6]^{9-}$ octahedra (Figure 2). The octahedra form a three-dimensional network by sharing edges among themselves (Figure 3). However, the $[PO_4]^{3-}$ tetrahedra are completely independent and share four of their O atoms with different neighboring $[BiO_6]^{9-}$ octahedra, as shown in Figure 4. As observed in the previously published crystal structures of eulytites, pentagonal channels, formed by packing of $[PO_4]^{3-}$ tetrahedra, were observed along the ⟨001⟩ direction (Figure 5).[27,30,36,38−40] In spite of the structural similarities, the local cationic and anionic environment is significantly diverse and eulytites have been divided into four categories, on the basis of this diversity.[39] In an earlier study, it was pointed out that eulytites show significant differences in the local environment, in particular by suggesting one, two, and three possible positions for oxygens.[38] Further, there have been ambiguities in the location of oxygen positions which obviously relate to the evolution of physical properties in these series of compounds. Most of the structures reported in this series show considerable difficulty in obtaining single crystals due to incongruent melting and inherent disorder. Figure 6 illustrates the variability of the nature of the oxygen environment in both ordered and disordered eulytites, available in the literature along with the structures studied by us.

The bond distances and angles present in these eulytites are consistent with the expected values of P−O and A/Bi−O and O−P−O and O−A/Bi−O, respectively, for this family of compounds. For $Ca_3Bi(PO_4)_3$, P−O1 and P−O2 bond

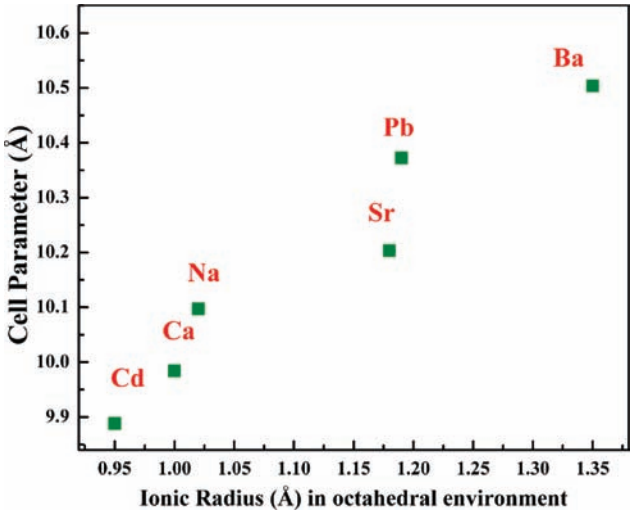

Figure 1. Change in cell parameters of phosphate eulytites as a function of ionic radii.

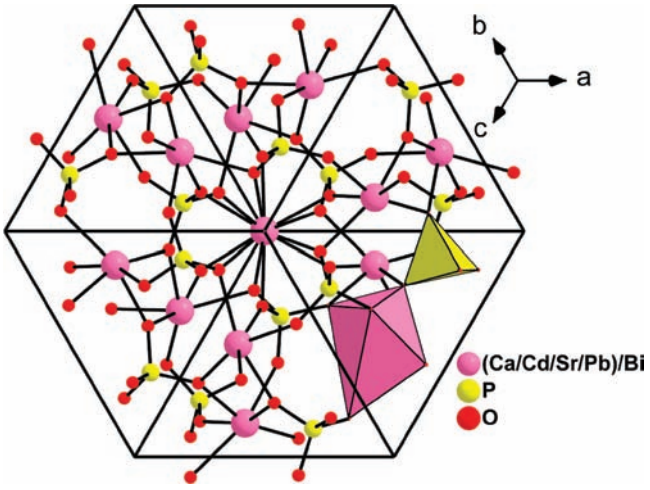

Figure 2. Three-dimensional view of eulytite structural type.

distances are 1.508(13) and 1.533(5) Å, respectively. The O1−P−O1 and O2−P−O2 bond angles deviate significantly from the ideal tetrahedral angle of 109.48°. There are two types of angles present in the tetrahedra: 113.2(3) ° and 107.62(15) ° for O1−P−O1 and 113.8(12) ° and 107.4(6) ° for O2−P−O2. The Ca/Bi sites have three short distances and three long distances with each oxygen atom. They are 2.271(4) and 2.443(5) Å for Ca/Bi−O1 and 2.382(17) and 2.74(3) Å for Ca/Bi−O2, respectively. For $Cd_3Bi(PO_4)_3$, the P−O1 and P−O2 bond distances are 1.514(14) and 1.51(7) Å, respectively. The tetrahedral angles for O1−P−O1 are 116.8(10) and 105.9(5) ° and for O2−P−O2 are 116.0 (4) and 106.3 (19) °, respectively. The two types of bond lengths for Cd/Bi−O1 are 2.266(13) and 2.377(14) Å and are 2.35(6) and 2.72(7) Å for Cd/Bi−O2. Similarly, for $Sr_3Bi(PO_4)_3$, the P−O1 and P−O2 bond distances are 1.524(8) and 1.520(19) Å, respectively. The tetrahedral angles are 113.3(8) and 107.6(4) °, for O1−P−O1, and 110.5(16) and 108.9(8) °, for O2−P−O2, respectively. The two types of bond lengths for Sr/Bi−O1 are 2.599(18) and 2.405(14) Å and are 2.47(3) and 2.405(14) Å for Sr/Bi−O2. Similarly for $Pb_3Bi(PO_4)_3$, the P−O bond distance is 1.539(9) Å and the tetrahedral angles are 110.8(5) and 108.8(5) °. The Pb/Bi−O bond distances are 2.636(9) and 2.343(8) Å.

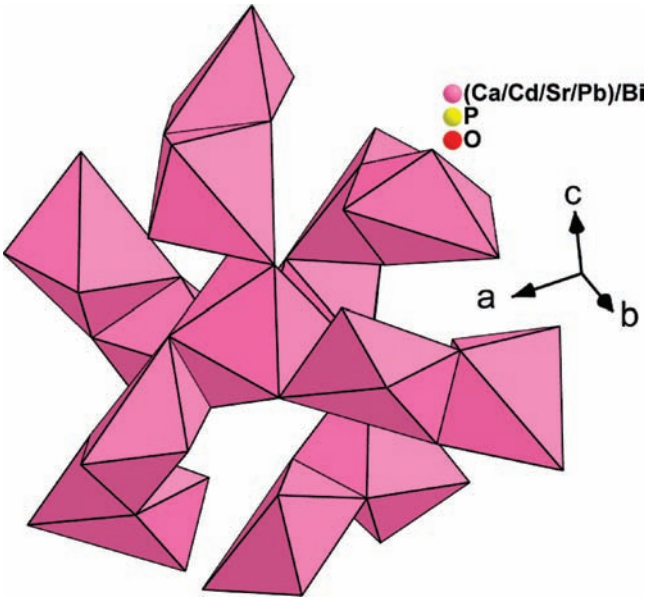

Figure 3. View of the structure depicting isolated $[PO_4]^{3-}$ tetrahedra.

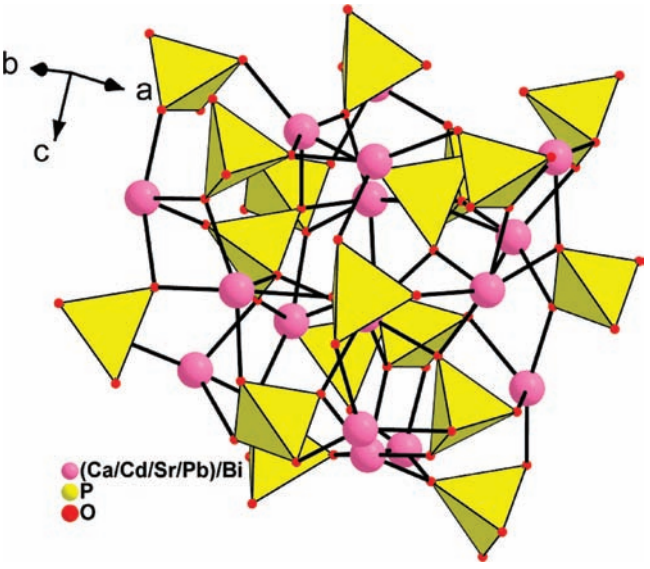

Figure 4. View of the structure showing edge shared A/Bi octahedra.

Laboratory and Variable Temperature Synchrotron XRD Data. The powder XRD patterns indicate the phase purity of the eulytites $Ca_3Bi(PO_4)_3$, $Pb_3Bi(PO_4)_3$, and $Sr_3Bi(PO_4)_3$. Profile refinements on the powder XRD data were carried out using *JANA2000* using the structural models obtained from single-crystal data. The experimental, calculated, and difference powder XRD profiles are presented in Figure 7. However, monophasic polycrystalline samples could not be prepared for the $Cd_3Bi(PO_4)_3$ and $Pb_3Bi(VO_4)_3$ eulytites. Additional phases of $Cd_3(PO_4)_2$ and $Pb_{2.5}Bi_{1/3}V_2O_8$ were present for the eulytites $Cd_3Bi(PO_4)_3$ and $Pb_3Bi(VO_4)_3$, respectively.[48,49] Rietveld refinements were carried out for $Pb_3Bi(VO_4)_3$, using the single-crystal structure, reported previously.[40] The percentage of the parasitic phase,

(48) Bigi, A.; Foresti, E. B.; Gazzano, M.; Ripamonti, A.; Roveri, N. *J. Chem. Res.-S* **1986**, 170.
(49) Sahoo, P. P.; Gaudin, E.; Darriet, J.; Row, T. N. G. *Inorg. Chem.* **2010**, *49*, 5603.

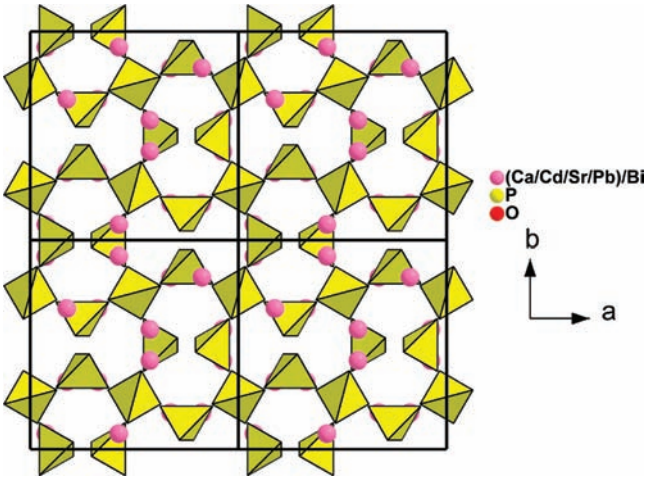

Figure 5. Three-dimensional view of eulytite along ⟨001⟩ showing pentagonal channels formed by $[PO_4]^{3-}$ tetrahedra.

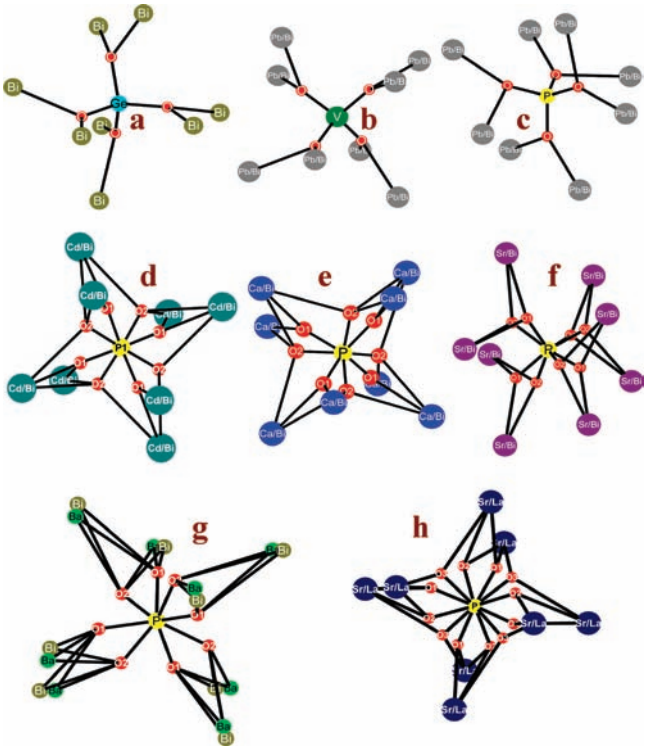

Figure 6. Coordination environment in different eulytites (a) $Bi_4(GeO_4)_3$, (b) $Pb_3Bi(VO_4)_3$, (c) $Pb_3Bi(PO_4)_3$, (d) $Cd_3Bi(PO_4)_3$, (e) $Ca_3Bi(PO_4)_3$, (f) $Sr_3Bi(PO_4)_3$, (g) $Ba_3Bi(PO_4)_3$, and (h) $Sr_3La(PO_4)_3$.

$Pb_{2.5}Bi_{1/3}V_2O_8$ for the eulytite, $Pb_3Bi(VO_4)_3$ was found to be approximately 5%. Rietveld refinements could not be carried out for $Cd_3Bi(PO_4)_3$, because of the complexity of the structure of the surrogate phase $Cd_3(PO_4)_2$.[48] Thus, profile refinements were carried out for $Cd_3Bi(PO_4)_3$. The experimental, calculated, and difference powder XRD profiles of $Pb_3Bi(VO_4)_3$ and $Cd_3Bi(PO_4)_3$ are presented in Figure 8.

Variable-temperature synchrotron powder XRD data from 398 to 100 K were collected for all the eulytites to investigate the possibility of any phase transition from the cubic phase. It was found that, in the case of $Pb_4(PO_4)_2CrO_4$, a low-temperature rhombohedral type phase was indicated at around 700 °C.[31] For all the compounds, no phase transitions were observed down to 100 K. Figure S2 in the Supporting Information indicates the absence of phase transitions for these compounds.

Single-Crystal Growth Characteristics. Growing single crystals of eulytites has always been a challenge, owing to their incongruent melting character augmented with thermal instabilities. Indeed, in cases where crystals were grown, the yield turned out to be always small. It appears from the above experiments that the use of the melt−cool technique is superior to the use of the flux method for quantitative yield and phase purity of eulytites. In fact, the yield of single crystals of $Pb_3Bi(PO_4)_3$ is almost 100% as compared to the yield of less than 5%, as reported previously using the flux method.[36] This 100% yield is a consequence of $Pb_3Bi(PO_4)_3$ displaying a sharp congruent melting point. However, the other eulytites melted incongruently. For example, $Ca_3Bi(PO_4)_3$ melts incongruently, generating an additional phase $Ca_3(PO_4)_2$ as shown in Figure S3 (Supporting Information). $Cd_3Bi(PO_4)_3$ melts incongruently at 1100 °C giving a few single crystals of the eulytite phase along with polycrystalline $Cd_3(PO_4)_2$ and $BiPO_4$, as shown in Figure S4 (Supporting Information). The eulytite phase $Cd_3Bi(PO_4)_3$ is very unstable and transforms to $Cd_3(PO_4)_2$ and $BiPO_4$ spontaneously with changes in temperature and pressure. However, good quality single crystals of the eulytite phase could be identified under the polarizing microscope and were picked for data collection. Likewise, $Pb_3Bi(VO_4)_3$ melts at 775 °C to result in a three component mixture of $Pb_3Bi(VO_4)_3$, palmierite type $Pb_{2.5}Bi_{1/3}V_2O_8$ and $BiVO_4$ (Figure S5 in the Supporting Information). The polycrystalline mixture transforms completely to the other two phases upon further heating to 800 °C. The powder XRD pattern of $Sr_3Bi(PO_4)_3$ after melting is more complex and forms a multiphasic mixture of $BiPO_4$, $Sr_3P_2O_8$, $Sr_2P_2O_7$, and $Sr_3Bi(PO_4)_3$ (Figure S6 in the Supporting Information). Such behavior was also observed in the case of $Ca_3Y(PO_4)_3$ and also for $Pb_3V(PO_4)_3$.[26,27,29] The systematic analysis of the melting characteristics followed by crystal growth of the eulytites clearly brings out the difficulties to obtain quality single crystals for X-ray diffraction study.

UV−Vis and Second Harmonic Generation Measurements. Room temperature UV−vis spectra were collected in the diffuse reflectance mode for various eulytites. The diffuse reflectance spectra were converted to absorbance like spectra using the Kubelka−Munk function (Figure 9). The compound $Pb_3Bi(VO_4)_3$ shows a lower band gap compared to the rest of the eulytites. The band gaps were calculated to be 2.5, 3.7, 4.0, 4.2, and 3.9 eV for $Pb_3Bi(VO_4)_3$, $Pb_3Bi(PO_4)_3$, $Sr_3Bi(PO_4)_3$, $Ca_3Bi(PO_4)_3$, and $Cd_3Bi(PO_4)_3$. The lower band gap for the vanadate eulytite, compared to the phosphate eulytites, is expected because of the presence of the $[VO_4]^{3-}$ moiety. It may be argued that, when the $[VO_4]^{3-}$ anion is combined with a cation, the energy of the charge transfer excitation decreases, hence resulting in a decrease in band gap.[50] For example, the band gap of $BiPO_4$ is 3.85 eV[51] whereas the vanadate analogue $BiVO_4$ has a band gap of 2.4−2.8 eV.[50] In the case of the phosphate eulytites, Pb containing

(50) Stoltzfus, M. W.; Woodward, P. M.; Seshadri, R.; Klepeis, J. H.; Bursten, B. *Inorg. Chem.* **2007**, *46*, 3839.
(51) Pan, C. S.; Zhu, Y. F. *Environ. Sci. Technol.* **2010**, *44*, 5570.

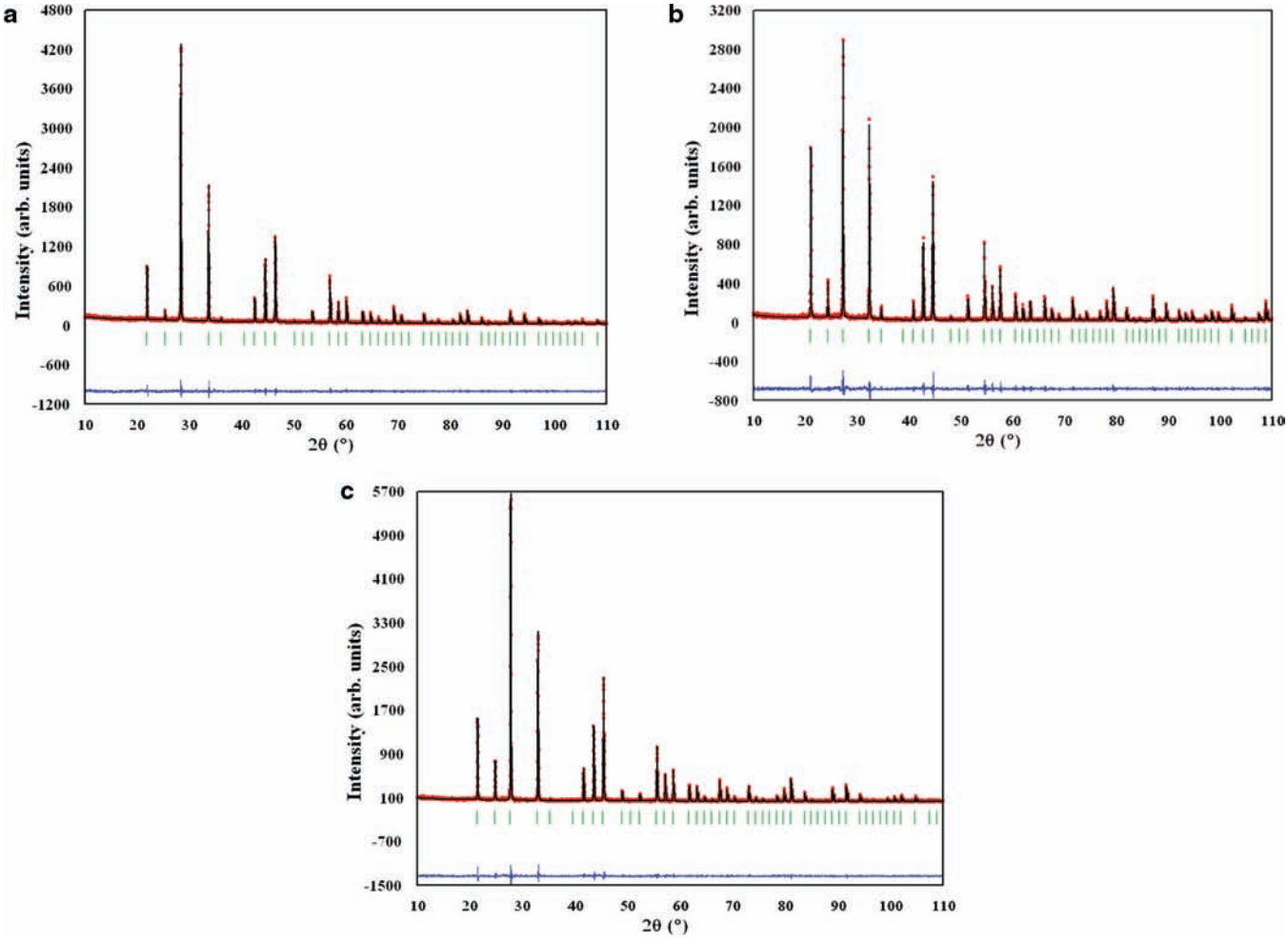

Figure 7. Experimental, calculated, and difference powder XRD diffraction profiles for (a) $Ca_3Bi(PO_4)_3$, (b) $Pb_3Bi(PO_4)_3$, and (c) $Sr_3Bi(PO_4)_3$.

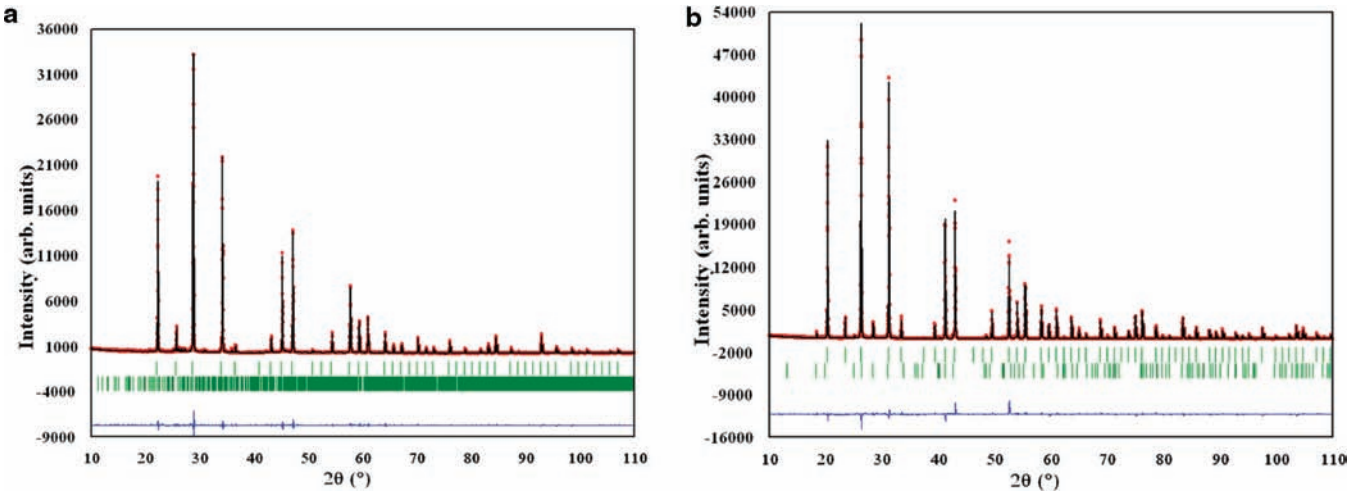

Figure 8. (a) Full pattern matching of the powder pattern of $Cd_3Bi(PO_4)_3$. The upper and lower rows of vertical marks correspond to the allowed reflections for $Cd_3Bi(PO_4)_3$ and $Cd_3(PO_4)_2$, respectively. (b) Full pattern matching of the powder pattern of $Pb_3Bi(VO_4)_3$. The upper and lower rows of vertical marks correspond to the allowed reflections for $Pb_3Bi(VO_4)_3$ and palmierite type $Pb_{2.5}Bi_{1/3}V_2O_8$, respectively.

eulytite has a lower band gap compared to the rest. The "$6s^2$" lone pairs of Pb are responsible for the lowering of the band gap.[36,50] In the literature, the electronic band structures of the eulytites, BGO, BSO, and $Pb_3Bi(PO_4)_3$ have been discussed. The calculations reveal the indirect band gap nature for all the eulytites studied. The electronic properties of the eulytites are more dominated by Pb/Bi−O interactions.[21,36,52]

(52) Lima, A. F.; Souza, S. O.; Lalic, M. V. *J. Appl. Phys.* **2009**, 106.

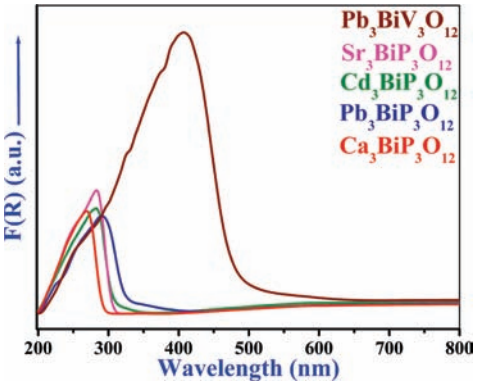

Figure 9. UV−vis diffuse reflectance spectra for various eulytites.

SHG measurements were carried out on the powder samples of all eulytites studied above (Kurtz−Perry method) at room temperature. For the compounds $Cd_3Bi(PO_4)_3$ and $Pb_3Bi(VO_4)_3$, the SHG measurements were performed on the polycrystalline samples with less than 5% of the secondary phases, because of the nonavailability of sizable amount of single crystals to grind and perform the measurements. The SHG measurements on the polycrystalline samples revealed that the intensity produced by these samples exhibit SHG efficiencies of about 5.3, 3.8, 2.85, 1.21, and 0.64 times that shown by KDP (KH_2PO_4) for $Pb_3Bi(VO_4)_3$, $Cd_3Bi(PO_4)_3$, $Sr_3Bi(PO_4)_3$, $Pb_3Bi(PO_4)_3$, and $Ca_3Bi(PO_4)_3$, respectively. However, in a recent report, $Pb_3Bi(PO_4)_3$ has been shown to exhibit an SHG activity 3.0 times in magnitude compared to that of KDP with increased particle size. This work also reports that this compound can be classified as a phase matching material.[36]

Conclusions

Crystal structures of several eulytites belonging to the family $A_3Bi(XO_4)_3$ (X = V, A = Pb; X = P, A = Ca, Cd, Sr, Pb) have been analyzed unequivocally by single-crystal XRD studies. All crystals were obtained by the melt−cool technique, and the incongruent melting behavior had been analyzed. The single-crystal analyses reveal the disorder in the cation and anion sublattices. The SHG measurements performed on these eulytites display prominent activity with respect to commercially available KDP, which makes them potential candidates for possible materials application.

Acknowledgment. P.P.S. thanks the Indian Institute of Science for a senior research fellowship. We acknowledge funding (SR/S1/IC-13/2008) from DST-India. We thank DST-FIST (level II) for funding the Oxford diffraction X-ray facility. We thank Professor P. K. Das, Department of Inorganic and Physical Chemistry, Indian Institute of Science, for providing SHG measurements. P.P.S. would like to thank DST-India and ICTP-Elettra user program for financial support during synchrotron data collection at Trieste, Italy. Thanks are due to Dr. Polentarutti Maurizio and Dr. Bais Giorgio for scientific assistance during synchrotron data collection.

Supporting Information Available: CIF: CIF's for the single-crystal XRD; single-crystal images of various eulytites (Figure S1); temperature evolution of various eulytites (Figure S2); full pattern matching of the powder pattern of $Ca_3Bi(PO_4)_3$ after melting at 1400 °C (Figure S3); full pattern matching of the powder pattern of $Cd_3Bi(PO_4)_3$ after melting at 1100 °C (Figure S4); full pattern matching of the powder pattern of $Pb_3Bi(VO_4)_3$ after melting at 775 °C (Figure S5); full pattern matching of the powder pattern of $Sr_3Bi(PO_4)_3$ after melting at 1450 °C (Figure S6). This material is available free of charge via the Internet at http://pubs.acs.org.